Turkish Journal of Electrical Engineering & Computer Sciences

http://journals.tubitak.gov.tr/elektrik/

Research Article

Turk J Elec Eng & Comp Sci
(2020) 28: 693 – 707

doi:10.3906/elk-1903-157

Optimal design of a flux reversal permanent magnet machine as a wind turbine generator

Majid GHASEMIAN, Farzad TAHAMI*, Zahra NASIRI-GHEIDARI
Department of Electrical Engineering, Sharif University of Technology, Tehran, Iran

Received: 26.03.2019 • **Accepted/Published Online:** 23.09.2019 • **Final Version:** 28.03.2020

Abstract: Flux reversal permanent magnet generators are well suited for use as wind turbine generators owing to their high torque generation ability and magnetic gear. However, they suffer from poor voltage regulation due to their high winding inductance. In this paper, a design optimization method is proposed for flux reversal generators in wind turbine applications. The proposed method includes a new multiobjective function. Cost, volume of the generator, and mass of the permanent magnet are considered in it independently and simultaneously. Besides the new objective function, the main superiority of this paper compared with published papers is considering winding inductance in optimization procedures as a constraint and analyzing the optimization results for different values of it. Also, for the first time, the equations for permanent magnet sizing are considered based on a demagnetization curve for designing a flux reversal generator. For this purpose, a step-by-step design procedure is proposed and sensitivity analysis is performed to determine the sensitivity of output parameters to specific electrical loading, the height of the permanent magnets, and the machine length-to-diameter ratio. Then a multiobjective optimization based on a genetic algorithm is carried out and the best combination of pole number and number of slots/pole/phase is obtained. Then, for this combination, the optimum value of the constraint is obtained, too. Then specifications and dimensions of the optimum flux reversal machine as a wind turbine generator is presented. Finally, a time-stepping finite element method is used to validate the design and optimization results.

Key words: Flux reversal generator, permanent magnet, wind turbine, optimization, inductance, demagnetization

1. Introduction

Today, numerous industrial applications such as ship propulsion, wind, and tidal power generation require high-torque low-speed drives, which often run below 150 rpm [1, 2]. Direct drive turbines have been used for avoiding gearboxes failures, reducing mechanical loss, increasing reliability, and lowering maintenance costs. The appropriate generators for such applications should have high torque generation ability. Permanent magnet (PM) machines are usually the most common and popular options in this field and flux reversal machines (FRMs) are new versions of these machines. An FRM is classified as a high-power density machine that operates based on the flux modulation effect between the stator teeth and rotor poles [3]. When the rotor rotates one turn, the winding flux linkage varies Zr times, where Zr is the number of rotor teeth. Hence, the winding flux variation in FRMs is faster than the rotor field rotation, which is known as the electromagnetic gearing effect. This kind of machine is a well-suited direct-drive application where the rotational speed is low. In an FRM, when the rotor rotates by one pole pitch, the polarity of the PM flux linkage in the armature winding is reversed, which is called "flux reversal".

*Correspondence: tahami@sharif.edu

The first group has concentrated on analyzing different aspects of FRM machines. For example, FRMs have an "electrical gear" property, which was introduced in [4] for the first time. In these machines, FRMs are analyzed with the combination of this concept and the conventional PM synchronous machine (PMSM) analysis methods. The d-q model of FRMs was developed in [5] based on the PMSM model and electrical gear concepts, where the power density of FRMs was increased with full pitch winding. In [6, 7] a subdomain model was developed for no-load and on-load magnetic field distribution calculation. The work in [8] focused on the harmonic content of back electromotive force by field modulation theory. Some of these papers have dealt with analyzing the different topologies of FRMs, such as transverse flux or linear form [9–11].

The second group has focused on designing FRMs. The first FRM, which was introduced in 1955, had a single-phase configuration [12]. The drawbacks of the single phase led researchers to introduce a three-phase FRM [13]. Since then, many studies have been done on the design and improvement of three-phase FRMs. The authors in [14] proposed using a flux barrier in the rotor and in [15] proposed the asymmetric stator pole to reduce the flux leakage. A magnetless FRM was first designed in [16], in which a four-phase DC field was used instead of PM for providing excitation control ability. An improved configuration was introduced in [17–19] for cogging torque reduction.

All the above-mentioned papers have focused on the advantages of FRMs. Nevertheless, one of the main drawbacks of the FRM as a generator –- i.e. large winding inductance –- has not been considered thoroughly in the design. In this paper, the optimum selection of winding inductance is considered in the design and optimization of a 1.5 MW direct drive generator.

Moreover, minimizing the permanent magnet weight in the FRM is another point that has been left unnoticed in the literature. Rare earth magnets are among the most expensive parts of PM machines. In this study, design equations will be presented based on the demagnetization characteristics so that the volume of the PM will be minimized during the optimization process.

The remainder of this study is organized as follows. In Section 2, the analytical design approach is proposed and design steps of an FRM are presented. Also, some equations are presented for determining the main dimensions of an FRPM, the permanent magnets, and inductance. In Section 3, the effects of several parameters on machine characteristics are investigated. In Section 4, the machine is optimized with a specific objective function. Finally, the validity of the design and optimization are investigated in Section 5 using time-stepping finite element analysis.

2. Analytical design method

In order to design a machine, it is necessary to determine four basic elements: input data, design procedure, assumptions, and outputs.

2.1. Input data

Input variables usually include generator rated values, material specification, and operational data. The purpose of this research is designing a gearless direct-drive wind generator. The widely used 1.5 MW 690 V generator class with a rated rotational speed of 19.65 rpm is considered for this purpose. Table 1 illustrates the generator rated values and specifications of the materials.

2.2. Design procedure

The design procedure is divided into three parts. First, the main machine dimensions are determined, and then the PM sizing is accomplished. Finally, the winding inductance is calculated.

Table 1. Generator nominal value and used material specification.

Parameters	Symbol and unit	Value
Power	P_n, Mw	1.5
Voltage	V, v	690
Efficiency	$\eta, \%$	95
Power factor	PF	1
Speed	n_r, rpm	19.65
Winding factor	K_w	0.95
Lamination factor	K_l	0.95
Slot fill factor	K_{co}	0.7
Maximum temperature	Θ_m, C°	120
Steel saturation	B_{sat}, T	2
Core loss coefficient	$K_h, K_c, w/m^3$	187.8, 1.578
Copper resistivity	$r_{co}, \Omega m$	1.72×10^{-8}

2.2.1. Main dimension calculation

The design procedure is started based on the general active power equation [20]:

$$P_n = 3\eta PFEI, \tag{1}$$

Where η is the machine efficiency, PF is the operation power factor, and E is induced voltage, which is equal to $2\pi K_w f N_{ph}\phi_p$. K_w is the winding factor, f is the electrical frequency, N_{ph} is the number of winding turns per phase, and ϕ_p is the flux under each pole. By substituting this equation in (1) and defining B_{av} and ac as follows, the air-gap diameter (D_g) and machine length (L) can be obtained from (4) by taking Y as the machine stack length to the air-gap diameter:

$$B_{av} = \frac{P\phi_p}{\pi D_g K_l L}. \tag{2}$$

B_{av} is the specific magnetic loading, which is defined as the total flux per unit area over the surface of the armature periphery [20]. K_l is the lamination factor, which is determined according to the effective to actual length of the machine, and P is the pole number.

$$ac = \frac{6N_{ph}I}{\pi D_g}. \tag{3}$$

ac is the specific electrical loading, which is defined as the total number of armature conductors per armature periphery at the air gap [20].

$$D_g = \sqrt[3]{\frac{\sqrt{2}PP_n}{\pi^3 K_l K_w PF\eta B_{av} acY}}. \tag{4}$$

$$L = YD_g. \tag{5}$$

The stator teeth number (Q_s) is specified according to the machine pole number P and the number of slots per pole per phase q as follows:

$$Q_s = mqP. \tag{6}$$

The rotor teeth number (Z_r) should be equal to:

$$Z_r = Q_s - \frac{P}{2}. \tag{7}$$

The machine stator yoke height h_{sy} and rotor yoke height h_{ry} are determined according to the flux under each pole and maximum permissible flux density for the electrical steel. Also, for optimum use of the PM material, the height of the rotor and stator yoke should be larger than the PM segment width.

$$h_{sy} = h_{ry} = \frac{\pi D_g B_{av} K_l}{2PB_{sat}}. \tag{8}$$

Slot dimensions are determined based on the space needed for copper wires:

$$A_s = \frac{A_{co} N_{cs}}{K_{co}}, \tag{9}$$

where K_{co} is the slot fill factor, which is related to the insulation type and winding technology; N_{cs} is the number of conductors per slot; and A_{co} is the cross-section area of each conductor that is calculated as follows:

$$N_{cs} = \frac{\pi D_g ac}{3IPq}, \tag{10}$$

$$A_{co} = \frac{r_{co} L_{co}}{R_{co}}, \tag{11}$$

where r_{co} is the copper resistivity, L_{co} is the total length of winding per phase, and R_{co} is the winding resistance per phase, calculated as follows:

$$L_{co} = (L + T_c) N_{cs} Pq, \tag{12}$$

$$R_{co} = \frac{P_{co}}{3I^2}. \tag{13}$$

T_c is the winding pole pitch and P_{co} is the allowable machine copper loss.

Finally, the slot width (W_{ss}) and slot height (Hs) are calculated as follows:

$$W_{ss} = \frac{\pi(D_g + 2h_m)}{Q_s} - W_{st}, \tag{14}$$

$$H_s = \frac{A_s}{W_{ss}}. \tag{15}$$

W_{st} is the stator tooth width, which is equal to $0.75 W_{pm}$ [13], where W_{pm} is the PM width.

2.2.2. PM dimension calculation

Irreversible demagnetization can occur by an opposite magnetic field with an intensity higher than magnet coercive force (H_c). Such a situation can occur due to excess current in the stator windings during a short

circuit fault or even heavy overloading of the generator. As shown in Figure 1,[1] the coercive force decreases with temperature rise so the worst case, i.e. the value corresponding to the highest operating temperature (T_{max}), is considered.

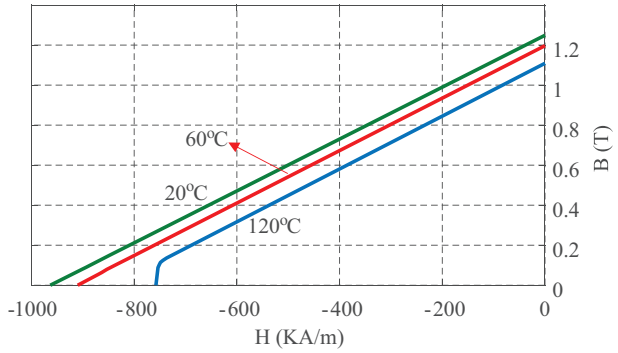

Figure 1. Demagnetization curve of PM - N38SH.

The equations for calculating the size of a PM were developed by Gieras in [21]. The minimum thickness of the magnet along the radial direction is determined by the armature reaction and demagnetization curve as follows:

$$h_{m-min} = \frac{K_a K_m F_{ad}}{H_c(T_{max})}, \tag{16}$$

where K_a is a safety factor that is set to 1.1 [22]. K_m is the ratio of the maximum possible current during a short circuit or overload to the nominal current. F_{ad} is the mmf of the direct axis armature reaction per pole with nominal current and can be calculated as follows:

$$F_{ad} = \frac{m2\sqrt{2}}{\pi P} K_{ad} K_w N_{ph} i_d. \tag{17}$$

K_{ad} is the direct axis armature reaction factor that can be obtained by FEM simulation (i.e. 0.9).

2.2.3. Inductance calculation

The machine inductance is caused by armature reaction and flux leakage. It directly affects the machine voltage regulation and converter system, which makes it an important parameter in the design procedure. For avoiding the complexity of inductance calculation, the equation in [4] is used with a modification factor (K_f). This factor is used to consider the leakage and fringing flux and is estimated based on the FEM analysis (i.e. 1.1).

$$L_s = K_f \frac{\pi \mu_0 N_{ph}^2 D_g L}{2P^2(h_m + \mu_r g)}. \tag{18}$$

2.3. Assumptions

During the design procedure, some unknown parameters are needed to be determined based on past experiences like winding factor (K_w), lamination factor (K_l), and slot fill factor (K_{co}), which are shown in Table 1. These parameters are categorized as the design assumptions and can be modified during the simulation procedure and construction.

[1] Sintered Neodymium Iron Boron (NdFeB) Magnets. Website https://www.eclipsemagnetics.com/media/wysiwyg/brochures/neodymium_grades_data.pdf[accessed 10 5 2019].

2.4. Outputs

Output variables are some electrical parameters like output power and inductance and also the geometrical parameters including the stator and the rotor dimensions. Here, the volume of machine, the mass of materials used in a machine, power density, and winding inductance are considered as output parameters.

3. Sensitivity analysis

As described in the previous part, there are many initially assumed parameters in the design procedure that can affect the performance of the machine. To reach an optimal design, some of these parameters should be determined during an optimization process. For this purpose, a sensitivity analysis for the influence of some parameters like specific electrical loading (ac), machine length to air-gap diameter ratio (Y), and PM height (hm) on the output characteristics is performed. The rated values of the sample FRPM are shown in Table 1. In this design, the number of pole pairs is considered to be 6, a full pitch distributed winding is used, and the number of slots per pole per phase is considered to be 2.

3.1. Specific electrical loading

Figure 2 shows the effect of increasing the specific electrical loading on the output characteristics of the sample FRPM. At first, the values of h_m and Y are assumed to be constant and equal to 25 mm and 0.5, respectively. Figure 2a shows that the machine volume (VM) is decreased as the specific electrical loading is increased. Consequently, the mass of steel (M_{st}) is reduced as well in the same manner (Figure 2b). Although the volume of the machine is decreased, the mass of copper (M_{co}) is increased (Figure 2c). In fact, the number of winding turns is increased with an increase in ac. To have a constant efficiency, a conductor with a larger cross-section is needed, which leads to an increase in the mass of copper. With constant PM height, the mass of PM (M_{pm}) is reduced as well (Figure 2d). Figure 2e shows that an increase in power density (P_d) leads to the total mass being reduced. The winding inductance is related to the diameter, length, square of winding turns, and air gap length. As shown in Figure 2f, the inductance of winding is larger for a higher value of ac. It shows that the effect of winding turn increment is more than the effect of reduction in the diameter and length. The larger inductance can deteriorate the voltage regulation and needs a larger DC bus voltage in the power electronic converter to compensate for the inductive voltage drop. Thus, the specific electrical value is limited by the winding inductance.

3.2. Machine length to diameter ratio

Figure 3 shows the effect of increasing Y on the output characteristics of the sample FRPM. In this investigation, the values of ac and h_m parameters are assumed constant and equal to 30,000 A/m and 25 mm, respectively. As shown in Figure 3a, the volume of the machine is slightly increased. An increase in the mass of steel is observed as well (Figure 3b). Although the machine length is increased, the reduction in winding turns and winding pole pitch leads to the reduction in copper mass (Figure 3c). In the beginning, the reduction rate is steep and then is gradual. According to (4) and (5), it can be concluded that the mass of PM is proportional to the third root of Y. Thus, a bigger Y leads to more PM mass (Figure 3d). As shown in Figure 3e, initially, the reduction in mass of copper leads to more power density, but eventually the power density is decreased due to the increase in the steel and PM mass. As shown in Figure 3f, the machine reactance is decreased by

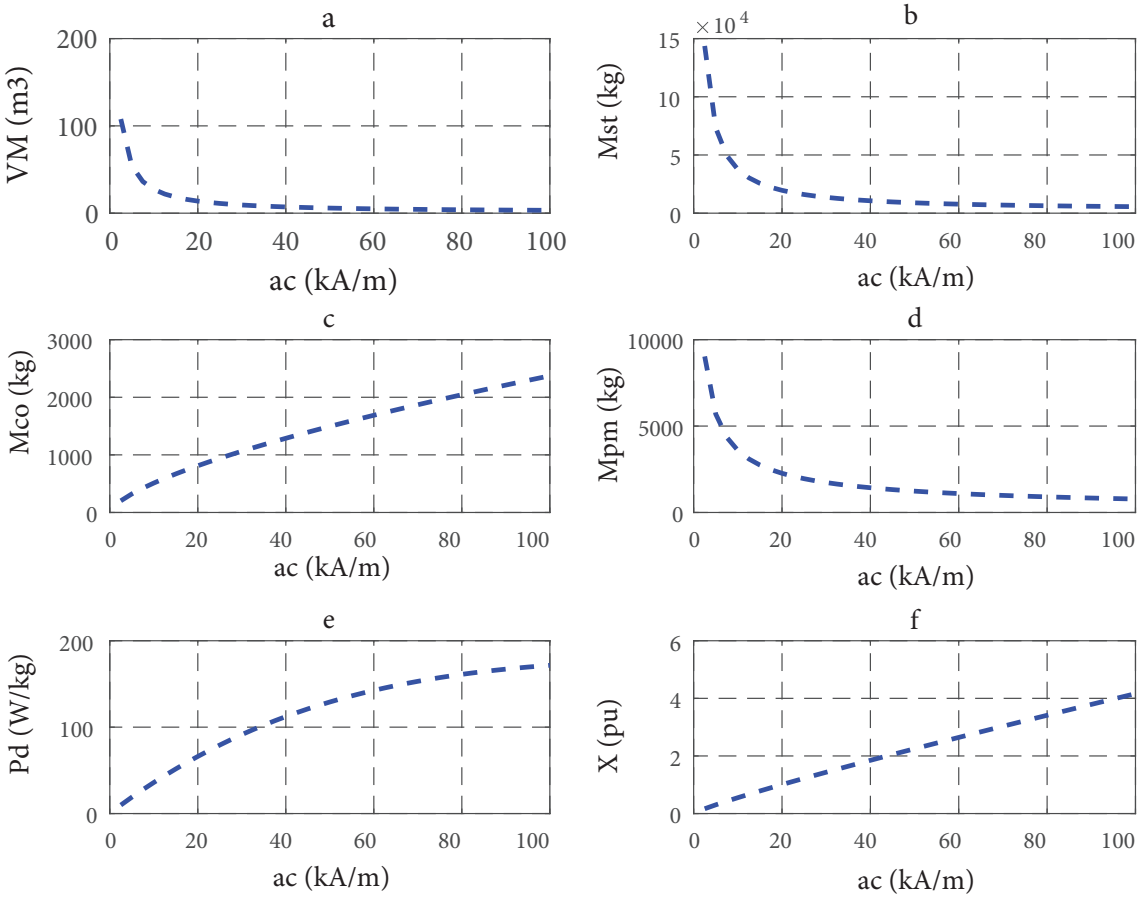

Figure 2. FRPM generator output characteristics versus *ac* parameter.

an increase in "Y". The bigger Y leads to fewer winding turns, smaller machine diameter, and lower winding reactance.

3.3. Permanent magnet height

In the previous parts, we presented the equations for calculating the minimum value of the PM height based on demagnetization characteristics. These equations only determine the minimum possible PM height and its exact value is determined during the design process. The output characteristics of the sample FRM are shown in Figure 4. The results are obtained with constant ac and Y equal to 30000 A/m and 0.5, respectively. As presented in Figure 4a and Figure 4b, by increasing the PM height, there is a slight increase in the machine volume and steel mass because of the increase in the machine outer diameter. Figure 4c shows that the copper mass is independent of the PM height and remains constant. As shown in Figure 4d, the mass of the PM is increased linearly such that there is an increase in the total mass of the machine and the power density of the machine is reduced (Figure 4e). The reluctance of the flux path is proportional to the PM height. Thus, the winding reactance is decreased with an increase in the PM height (Figure 4f). Therefore, an increase in the PM height has a positive role in reducing the winding reactance and power converter cost but will increase the overall machine cost. Hence, a compromise is needed to deal with this issue. In the next part, the optimization process will be presented to design an optimum FRM.

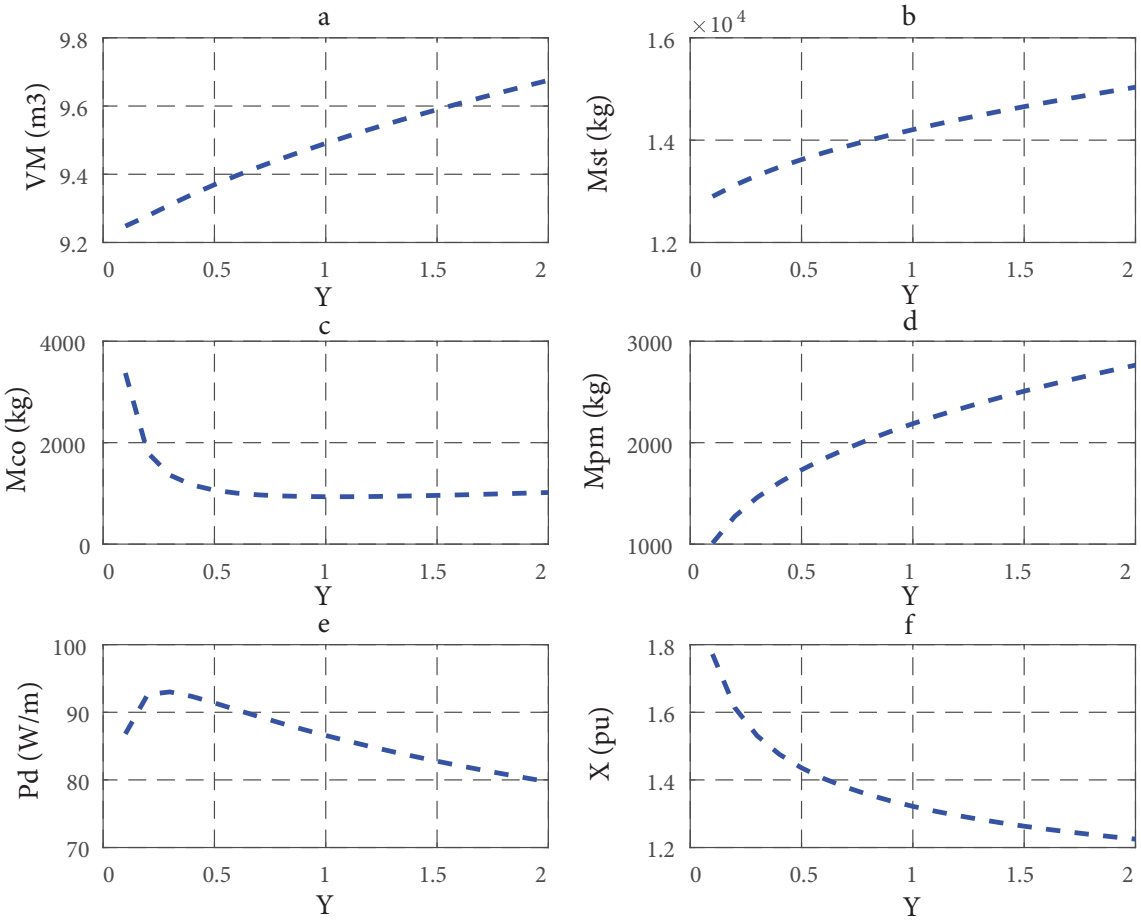

Figure 3. FRPM generator output characteristics versus Y parameter.

4. Optimization

Four steps are followed for optimization: 1) determining the optimization variables; 2) defining an objective function; 3) specifying the optimization constraints; and 4) presenting the optimization algorithm and analyzing the results.

4.1. Optimization variables

In this paper, the specific electrical loading, machine length-to-diameter ratio, and PM height are considered as optimization variables. X = x_1, x_2, x_3, where x_1=ac, x_2=Y, and x_3=h_m. The following ranges are considered during the optimization algorithm:

$$\begin{aligned} 1000 \leq x_1 \leq 100000(\frac{A}{m}), \\ 0.2 \leq x_2 \leq 2, \\ 8 \leq x_3 \leq 50(mm). \end{aligned} \tag{19}$$

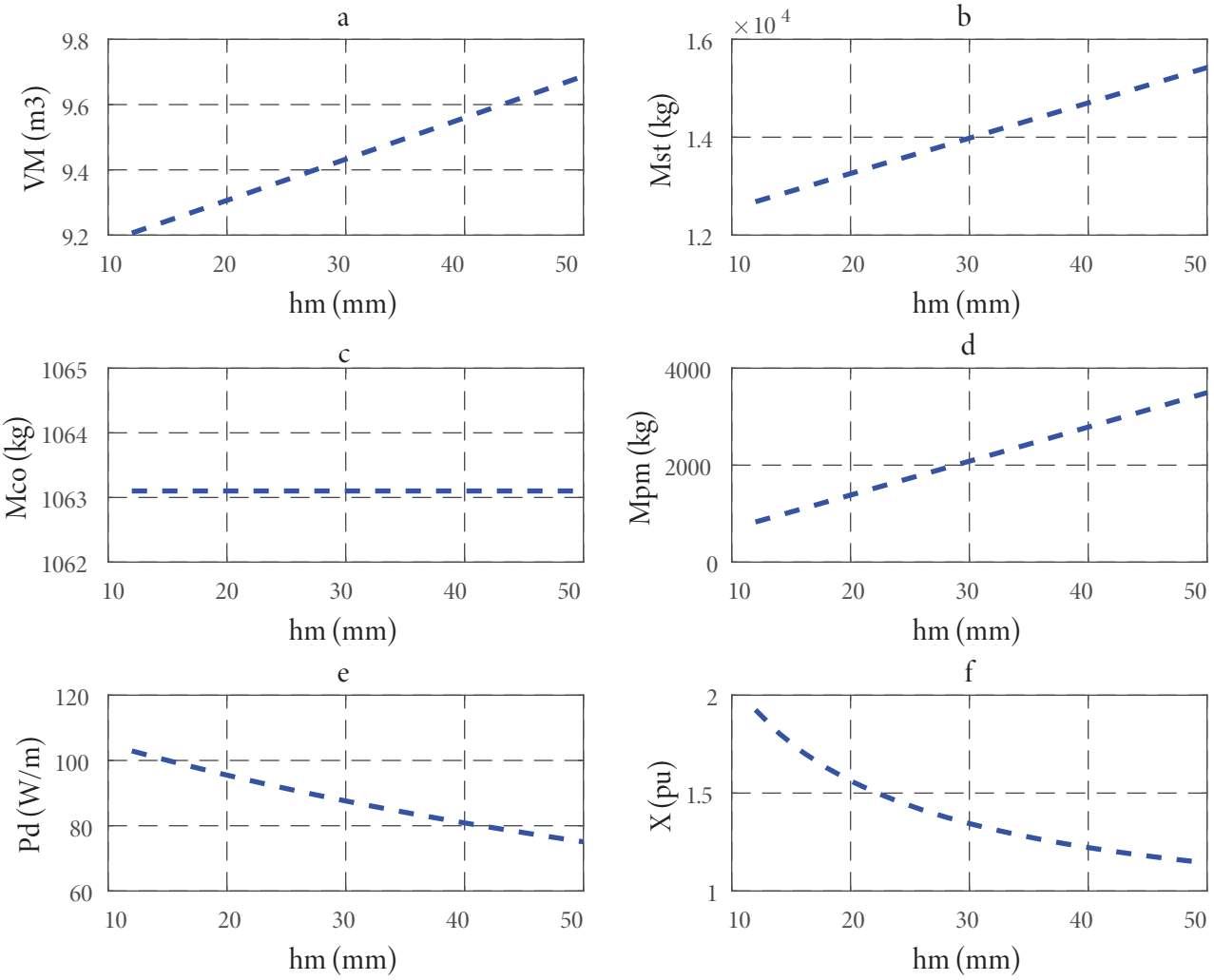

Figure 4. FRPM generator output characteristics versus h_m parameter.

4.2. Objective functions

The objective functions are used as a measure for the effectiveness of the design. An objective function can be a formulation of multiple objectives, which is known as multicriteria optimization. These criteria depend on design goals. The common criterion is the machine cost from the economic view. Here, the total cost of the materials including steel, copper, and magnet are considered as the first criterion for the objective function and is denoted by the symbol "cost". In the wind turbine application, according to the installation place, the generator size is sometimes more important than the machine price, so it is also considered as an object in the objective function and is denoted by V_M. The PM mass is the third object in the objective function from the feasibility view and is denoted by M_{pm}. These objectives are normalized based on the initial primary values and from the objective function as follows:

$$F(X) = \min(cost^{k1} V_M^{k2} M_{pm}^{k3}), \tag{20}$$

where K_i (i=1,2,3) is the weight assigned to each object for a different scenario. With different values of k_i, it is possible to consider each object separately or together. In the next sections, different scenarios will be investigated and the results will be presented.

4.3. Optimization constraints

Usually, the objective function is optimized based on some limits, which are known as optimization constraints that can be in equality or inequality forms. The winding reactance is a key parameter that determines the terminal voltage of the generator. With id=0 control, which is the common control method for the generator, and neglecting the winding resistance, the terminal voltage of the generator is approximately equal to $\sqrt{(1+X_{pu}^2)}$ (pu). Therefore, a big reactance can increase the generator terminal voltage. Thus, a constraint is set on the winding reactance as:

$$X_{pu} \leq X_{pu-max}. \tag{21}$$

According to (16), another limit on the optimization process is PM height, which is shown by $h_{m-min} \leq h_m$. Maximum operation temperature of the generator is another limit on each machine design, which is shown by $\Theta \leq \Theta_m$ and will be considered during the optimization process.

4.4. Optimization algorithm and results

The well-known genetic algorithm (GA) is used in this paper for finding the optimum solution in MATLAB. For finding the accurate answer, each optimization is repeated more than 100 times and the more repeated answer is chosen. The primary values of optimization variables are $ac = 15000$ A/m, $h_m = 15$ mm, and $Y = 0.5$. The results are shown with and without the constraint in Table 2. The value of X_{pu-max} is considered to be 1 pu.

Table 2. Optimization results.

Senario	Without constraint						With constraint			
$K1, K2, K3$	ac	h_m	Y	$F(X)$	X_{pu}	V_{pu}	ac	h_m	Y	$F(X)$
1,0,0	54000	14	0.9	0.453	3.2	3.35	13000	12	0.2	0.751
0,1,0	100000	27	0.2	0.171	4.27	4.4	29000	47	1.5	0.564
0,0,1	37000	7	1.6	0.427	2.35	2.55	13000	10	0.2	0.635
1,1,1	95000	20	0.6	0.039	4.15	4.26	13000	12	0.2	.0622

As the first scenario ($K1$=1, $K2$=0, $K3$=0), only the cost is considered in the objective function. The value of the objective function reaches 0.453. It is obvious that the higher value of ac and lower values for h_m and Y will result in a lower amount of high price PM and lower cost, but the value of these parameters are limited by the PM demagnetization condition. As shown in Table 2, in order to reduce winding reactance to 1 (pu) according to the optimization constraint, the values of variables are reduced and the objective function value is increased because of larger stator diameter and used material increment. In the second scenario ($K1$=0, $K2$=1, $K3$=0), only the generator volume is considered. As shown in Table 2, for reducing the volume, ac is increased and Y is reduced as much as possible, and the value of h_m is determined according to the demagnetization conditions, which results in $F(x) = 0.171$. To satisfy the optimization constraint, the value of ac is decreased and the values of h_m and Y are increased, which leads to an increase in $F(x)$ to 0.564. According to the third scenario ($K1$=0, $K2$=0, $K3$=1), only the mass of PM is important. Thus, the height of the PM is minimized

as much as possible and a value of 0.427 is obtained for $F(x)$. To satisfy the constraint on reactance, the value of $F(x)$ is increased to 0.635. In the fourth scenario ($K1$=1, $K2$=1, $K3$=1), all objectives are considered simultaneously. The value of $F(x)$ without considering constraints is equal to 0.039. With these parameters, the winding reactance and output voltage are 4.15 and 4.26 pu, respectively. The value of $F(x)$ increases to 0.0622 when satisfying the constraints.

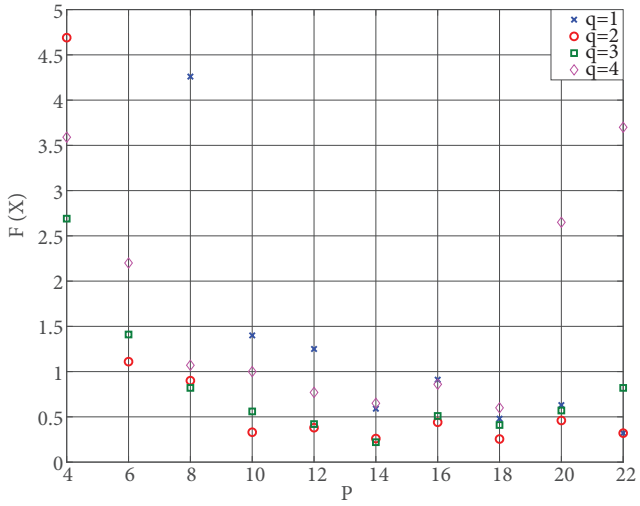

Figure 5. Minimum value of $F(X)$ for different combinations of P and q.

In all previous analyses, P and q are assumed to be 12 and 2, respectively. For completing the design procedure, different combinations of P and q are considered and the optimization process is repeated. Figure 5 shows the results of the optimization. It can be seen that the minimum value of the objective function is obtained with P and q equal to 14 and 3, respectively.

As shown in Table 2, the limitation on the reactance value has a deep impact on optimization results and must be selected optimally. For this purpose, the optimization process is repeated for different values of X_{pu-max}. Figure 6 shows a change in the generator volume and used materials versus X_{pu-ax}. The optimum point is obtained at $X_{pu-max} = 2$, where the machine volume and used materials' mass are minimum. The dimensions of the optimized generator are shown in Table 3.

Table 3. Optimized generator dimensions.

Parameters	Value	Parameters	Value	Parameters	Value
P	20	D_g	2530 mm	g	3 mm
q	3	L	1000 mm	W_{ss}	35 mm
Q_s	180	h_{sy}, h_{ry}	50 mm	H_s	65 mm
Z_r	170	h_m	9 mm	N_{cs}	1

5. Finite element analysis

In this section, the optimized generator is simulated and the results of the 2D finite element method (FEM) are presented for validating the optimization. Figure 7 shows the no-load three-phase induced voltage for the

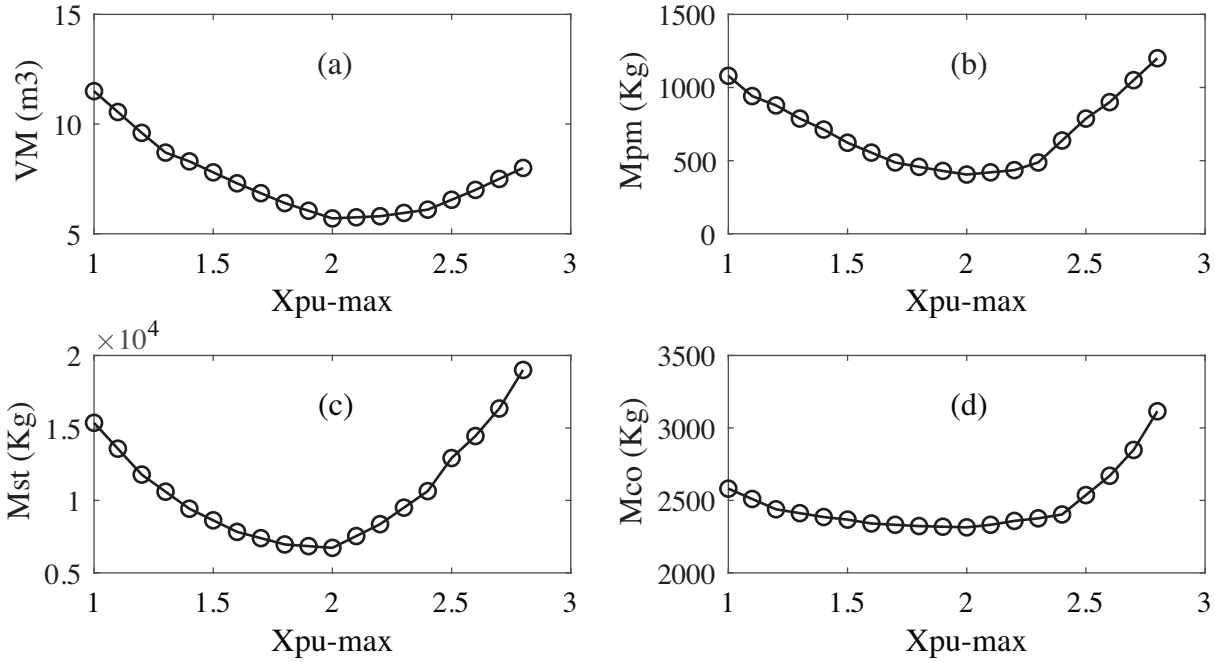

Figure 6. Change in generator value and used materials versus X_{pu-max}: a) generator volume, b) PM mass, c) steel mass, d) copper mass.

optimized generator. The amplitude of the induced voltage is equal to 560 V and that means 690 V-rms for the line-to-line voltage as considered for generator rated value.

The simulation results for the winding self and mutual reactance are shown in Figure 8. The sum of the self and mutual reactance is 0.95 pu, which conforms to the optimization constraint.

The output power of the optimized generator at nominal conditions and maximum operation temperature is shown in Figure 9a. As expected, the output power of the generator is equal to the rated value of 1.5 MW at the rated stator current. The ripple of output power is 2.6%. The cogging torque is plotted in Figure 9b, which has a peak to peak value lower than 0.15% of the nominal torque.

The distribution of the flux density under each pole of the optimized FRPM is shown in Figure 10. The flux density is less than 2 T in this area, which is lower than the saturation value as given in Table 1.

6. Conclusion

In this paper, the design and multiobjective optimization of an FRM as a wind turbine generator is proposed as a complete reference for designing this type of machine. In comparison with previous papers, this paper presented a novel optimization procedure with new multiobjective function by considering winding inductance as an optimization constraint and determining an optimized value for it. The sizing equations were presented considering the PM demagnetization curve and the winding inductance. The effects of several design parameters such as specific electrical loading, magnet thickness, and stack length on the output characteristics including volume of materials, power density, and winding inductance were investigated. Then the GA was used to find the optimal dimensions of the generator. The objective function, which included cost, volume, and mass of the PM, was optimized simultaneously and independently. The winding inductance limit was considered as a constraint during the optimization. The results showed that the inductance as a constraint could deteriorate

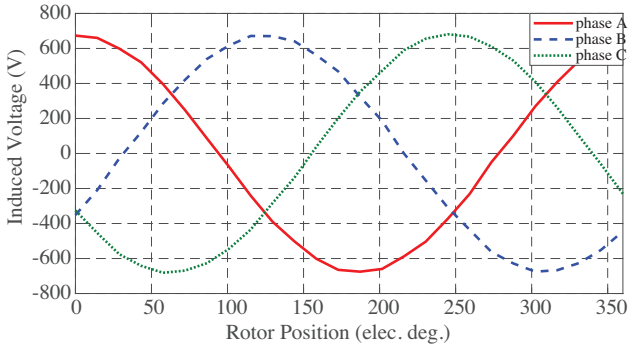

Figure 7. No-load induced voltage of the optimized generator.

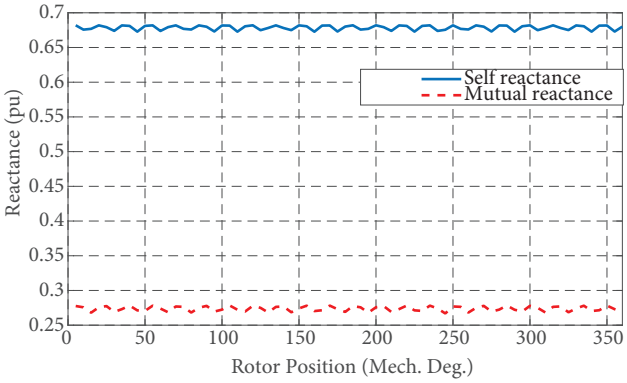

Figure 8. Winding self and mutual reactance.

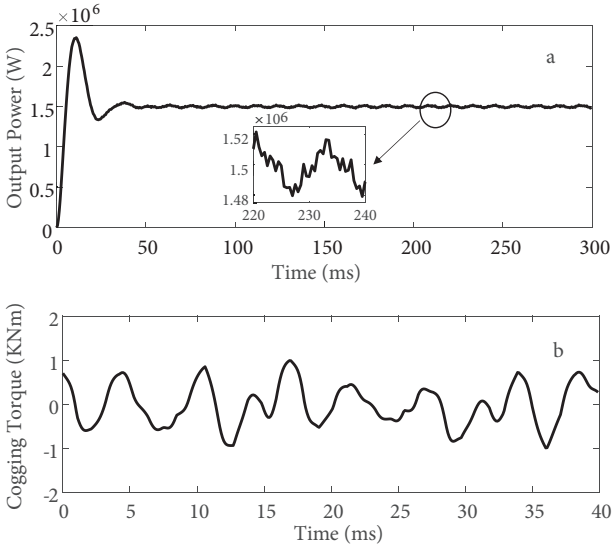

Figure 9. Output power and cogging torque of the optimum generator at nominal condition.

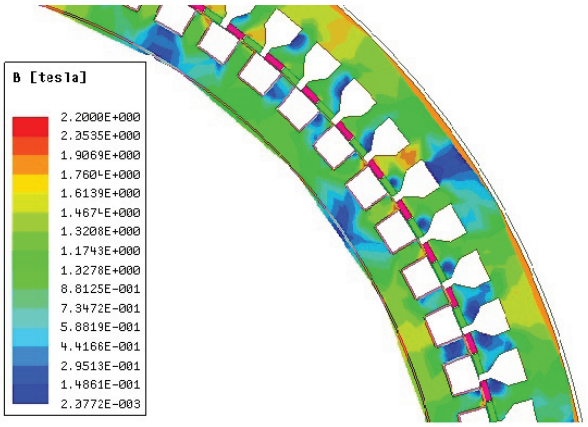

Figure 10. Flux density distribution of the optimum generator at nominal conditions.

the objective function value. As a result of optimization, the optimal values for the pole number and the number of slots/pole/phase were determined. The effects of constraints on generator volume and used materials were analyzed and the constraints were selected optimally. The results show that the optimum 1.5 MW FRM generator is obtained with winding reactance equal to 2 pu by a combination of 20 poles and number of slots/pole/phase equal to 3. The validity of the proposed design and optimization was verified by the time-stepping FEM. Results showed that the optimum generator has cogging torque less than 0.15% and generates the nominal power with ripple less than 2.6% at nominal conditions.

References

[1] Boldea I, Zhang L, Naser SA. Theoretical characterization of flux reversal machine in low-speed servo drives-the pole-PM configuration. IEEE Transactions on Industry Applications 2002; 37 (5): 1549–1556. doi: 10.1109/TIA.2002.804759

[2] Niu S, Ho SL, Fu WNA. Novel direct-drive dual-structure permanent magnet machine. IEEE Transactions on Magnetics 2010; 45: 2035-2039. doi: 10.1109/TMAG.2010.2041197

[3] Wu ZZ, Zhu ZQ, Zhan HL. Comparative analysis of partitioned stator flux reversal PM machines having fractional-slot nonoverlapping and integer-slot overlapping windings. IEEE Transactions on Energy Conversion 2016; 31: 776-788. doi: 10.1109/TEC.2016.2525826

[4] More DS, Fernandes BG. Analysis of flux-reversal machine based on fictitious electrical gear. IEEE Transactions on Energy Conversion 2010; 25: 940-946. doi: 10.1109/TEC.2010.2048330

[5] More DS, Fernandes BG. Modeling and performance of three-phase 6/14 pole flux reversal machine. IET Electric Power Applications 2013; 6 (2): 131-139. doi: 10.1049/iet-epa.2012.0058

[6] Yang Y, Wang X, Zhang Z. Analytical calculation of magnetic field and electromagnetic performance of flux reversal machines. IET Electric Power Applications 2014; 7 (5): 167-177. doi: 10.1049/iet-epa.2013.0187

[7] Guo K, Fang S, Lin H, Yang H, Huang Y. 3-D analytical analysis of magnetic field of flux reversal linear-rotary permanent-magnet actuator. IEEE Transactions on Magnetics 2016; 53 (5): 1-5. doi: 10.1109/TMAG.2017.2662079

[8] Zhu X, Hua W, Wang W, Huang W. Analysis of back-EMF in flux-reversal permanent magnet machines by air gap field modulation theory. IEEE Transactions on Industrial Electronics 2019; 66 (5): 3344-3355. doi: 10.1109/TIE.2018.2854575

[9] Xie K, Li D, Qu R, Yu Z, Gao Y. Analysis of a flux reversal machine with quasi-halbach magnets in stator slot opening. IEEE Transactions on Industry Applications 2019; 55 (2): 1250-1260. doi: 10.1109/TIA.2018.2873540

[10] Zhu S, Zheng P, Yu B, Cheng L, Fan Y. Performance analysis and modeling of a tubular staggered-tooth transverse-flux PM linear machine. Energies 2016; 9 (3): 163. doi: 10.3390/en9030163

[11] Kou B, Luo J, Yang X, Zhang L. Modeling and analysis of a novel transverse-flux flux-reversal linear motor for long-stroke application. IEEE Transactions on Industrial Electronics 2016; 63 (10): 5237-5247. doi: 10.1109/TIE.2016.2581142

[12] Rauch SE, Johnson LJ. Design principles of flux-switching alternators. Transactions of the American Institute of Electrical Engineers 1995; 74 (3): 1261–1268. doi: 10.1109/AIEEPAS.1955.4499226

[13] Boldea I, Nasar SA. Three phase flux reversal machine. IET Electric Power Applications 1999; 146 (2): 139–145. doi: 10.1049/ip-epa:19990114

[14] Kim TH, Lee J. A study of the design for the flux reversal machine. IEEE Transactions on Magnetics 2004; 40 (4): 2053–2055. doi: 10.1109/TMAG.2004.832488

[15] Yang H, Lin H, Zhu ZQ, Lyu S, Liu Y. Design and analysis of novel asymmetric-stator-pole flux reversal PM machine. IEEE Transactions on Industrial Electronics (in press). doi: 10.1109/TIE.2019.2896097

[16] Lee CHT, Chau KT, Liu C. Design and analysis of a cost-effective magnet less multi-phase flux-reversal DC-field machine for wind power generation. IEEE Transactions on Energy Conversion 2015; 30 (4): 1555-1563. doi: 10.1109/TEC.2015.2443155

[17] Zhu X, Hua W. An improved configuration for cogging torque reduction in flux-reversal permanent magnet machines. IEEE Transactions on Magnetics 2016; 53 (5): 1-1. doi: 10.1109/CEFC.2016.7816063

[18] Zhu X, Hua W, Wu Z. Cogging torque suppression in flux-reversal permanent magnet machines. IET Electric Power Applications 2017; 12 (1): 135-143. doi: 10.1049/iet-epa.2017.0342

[19] Li D, Gao Y, Qu R. Design and analysis of a flux reversal machine with evenly distributed permanent magnets. IEEE Transactions on Industry Applications 2017; 54 (1): 162-173. doi: 10.1109/TIA.2017.2750998

[20] Huang S, Luo J, Leonardi F, Lipo TAA. General approach to sizing and power density equations for comparison of electrical machines. IEEE Transactions on Industry Applications 1998; 34 (1): 92-97. doi: 10.1109/28.658727

[21] Gieras JF, Wing M. Permanent Magnet Motor Technology: Design and Application. 2nd edition. New York, NY, USA: Marcel Dekker, 2002.

[22] Mi C. Analytic design of permanent magnet traction drive motors. IEEE Transactions on Magnetics 2005; 42 (7): 1751-1755. doi: 10.1109/TMAG.2006.874511